

## CORONAL PSEUDOSTREAMERS

Y.-M. WANG, N. R. SHEELEY, JR., AND N. B. RICH<sup>1</sup>

E. O. Hulburt Center for Space Research, Naval Research Laboratory, Washington, DC 20375-5352;  
ywang@yucca.nrl.navy.mil, sheeley@spruce.nrl.navy.mil, nathan.rich@nrl.navy.mil

Received 2006 October 20; accepted 2006 December 1

### ABSTRACT

In a recent study of the 2006 solar eclipse, we noted that there are two kinds of coronal streamers: “helmet streamers,” which separate coronal holes of opposite magnetic polarity, and “pseudostreamers,” which overlie twin loop arcades and separate holes of the same polarity. It is well known that the heliospheric plasma and current sheets represent the outward extension of helmet streamers. Using white-light data from the Large Angle and Spectrometric Coronagraph (LASCO), we here show that pseudostreamers likewise have plasma sheet extensions, across which the polarity does not reverse; these multiple sheets contribute significantly to the brightness of the K corona, although their internal densities tend to be lower than those in the heliospheric plasma sheet. We use current-free extrapolations of photospheric field measurements to simulate the observed brightness patterns in the outer corona, including the contributions of both helmet streamer and pseudostreamer plasma sheets. Running-difference images show that pseudostreamers are relatively quiescent, resembling large-scale plumes; preliminary analysis suggests flow speeds as high as  $200 \text{ km s}^{-1}$  at heliocentric distances of only  $\sim 3 R_{\odot}$ , supporting the prediction (based on their low flux tube divergence rates) that pseudostreamers are sources of fast solar wind.

*Subject headings:* solar wind — Sun: corona — Sun: magnetic fields

### 1. INTRODUCTION

The close relationship between coronal streamer patterns and interplanetary sector boundaries has long been recognized (see, e.g., Hansen et al. 1974; Howard & Koomen 1974; Pneuman et al. 1978; Burlaga et al. 1981; Gosling et al. 1981; Wilcox & Hundhausen 1983; Wang et al. 2000; Liewer et al. 2001; Saez et al. 2005; Thernisien & Howard 2006). However, in studying the solar eclipse of 2006 March 29 (Wang et al. 2007), we realized that there are in fact two kinds of white-light streamers: (1) helmet streamers, which separate open field lines of opposite polarity; and (2) “pseudostreamers,” which separate open field lines of the same polarity. While both types of structures contribute to the brightness of the K corona, only the familiar helmet streamers are associated with interplanetary sector boundaries and the heliospheric current sheet (HCS).

The purpose of this paper is to further elucidate the properties of pseudostreamers. We begin by presenting some examples of observed pseudostreamers and deriving their magnetic topologies (§ 2). In § 3, we construct a simple model for the brightness distribution of the outer corona, including the contributions of both helmet streamers and pseudostreamers, and compare the simulated patterns with coronagraph observations. We conclude by discussing the physical nature of pseudostreamers and their outflows (§ 4).

### 2. EXAMPLES OF PSEUDOSTREAMERS

Figure 1 shows a pseudostreamer observed at the edge of the north polar coronal hole during the total eclipse of 2005 April 8. The figure represents a composite of a white-light picture taken at 21:15 UT,<sup>2</sup> and a He II 30.4 nm image recorded at 21:29 UT with the Extreme Ultraviolet Imaging Telescope (EIT; Delaboudinière 1995) on the *Solar and Heliospheric Observatory (SOHO)*. The

pseudostreamer is bounded on its poleward and equatorward sides by dark helium coronal holes. Other characteristic features are the low-lying cusp, in this case located  $\sim 0.25 R_{\odot}$  above the solar surface, and the presence of two underlying filament channels.

The magnetic topology of the pseudostreamer is displayed in Figure 2, where we have applied a potential-field source-surface (PFSS) extrapolation to the observed photospheric field for Carrington rotation (CR) 2028. In the PFSS model (Schatten et al. 1969), the magnetic field  $\mathbf{B}(r, L, \phi)$  remains curl free out to a spherical “source surface” at  $r = R_{ss} = 2.5 R_{\odot}$ , where the non-radial field components are set to zero; here  $r$  denotes heliocentric distance,  $L$  heliographic latitude, and  $\phi$  Carrington longitude. At  $r = R_{\odot}$ ,  $B_r$  is matched to the (nonpotential) photospheric field, which is taken to be radially oriented at the depth where it is measured (Wang & Sheeley 1992). All field lines that cross the source surface are defined as “open,” with their footpoint areas representing coronal holes. The magnetograph data employed in this study are from the Mount Wilson Observatory (MWO); we have corrected for the saturation of the Fe I 525.0 nm line profile by multiplying the field strengths by the latitude-dependent factor  $(4.5 - 2.5 \sin^2 L)$  (see Wang & Sheeley 1995; Arge et al. 2002; Ulrich et al. 2002).

From Figure 2, we see that the pseudostreamer is centered above a positive-polarity region that separates two coronal holes of negative polarity. The open field lines from the like-polarity holes converge above the closed field region, which overlies two photospheric neutral lines and thus contains a pair of loop arcades.

Figure 3 shows the outward extension of the pseudostreamer beyond  $r \sim 2 R_{\odot}$ , as it appeared at 07:27 UT on 2005 April 9. The image was recorded with the Large Angle and Spectrometric Coronagraph (LASCO; Brueckner et al. 1995) on *SOHO*; a background representing the contribution of the F corona and instrumental stray light has been subtracted. The structure is now oriented almost edge-on in the line of sight and forms a long, narrow spike. Note that the low-lying cusp of the pseudostreamer remains completely hidden behind the LASCO C2 occulting disk.

<sup>1</sup> Interferometrics, Inc., Herndon, VA.

<sup>2</sup> See <http://www.zam.fine.vutbr.cz/~druck/Eclipse>.

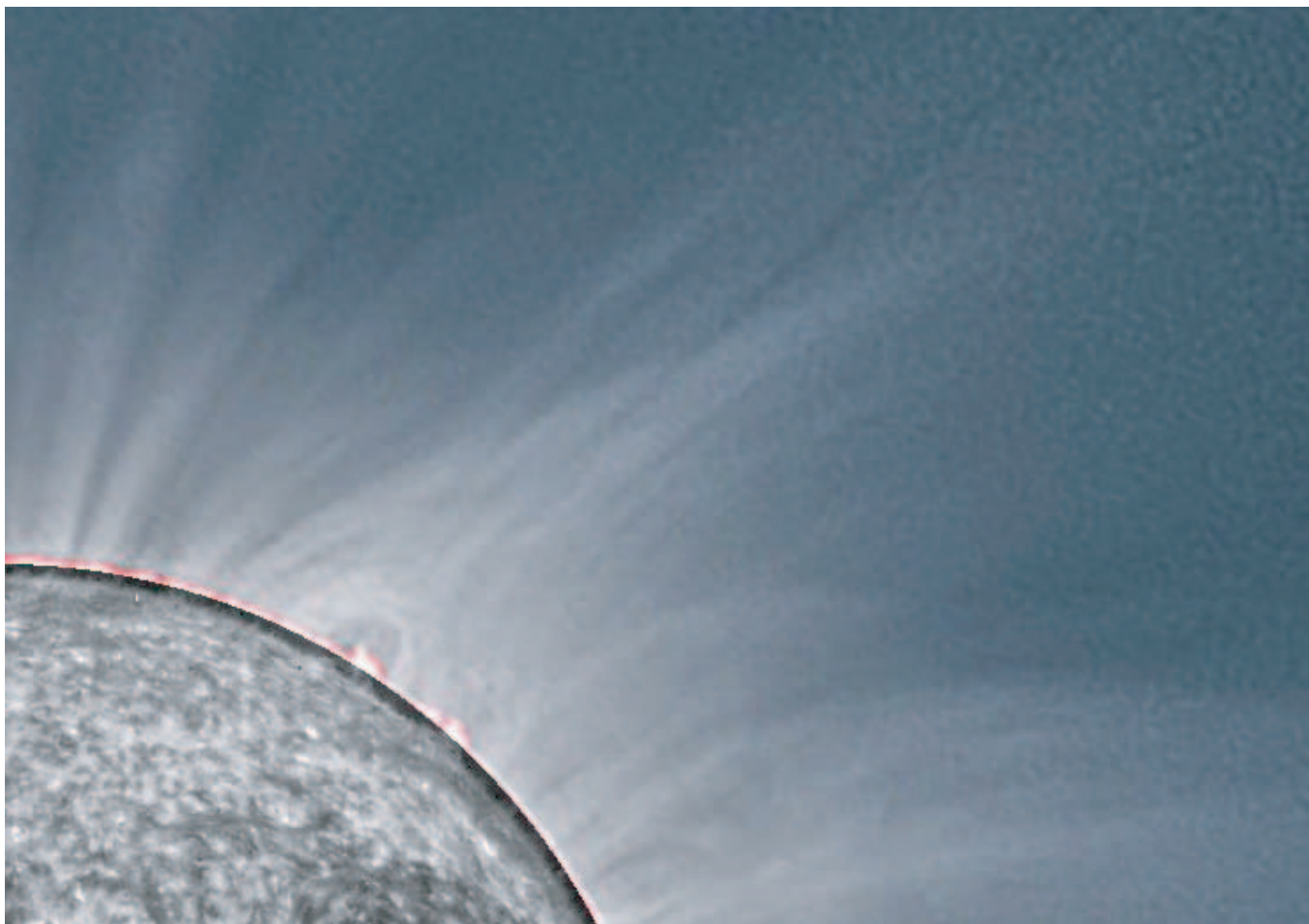


FIG. 1.—Pseudostreamer rooted at the western edge of the north polar coronal hole, 2005 April 8. Composite of a white-light eclipse picture taken at 21:15 UT and a He II 30.4 nm image recorded at 21:29 UT with *SOHO*/EIT. The pseudostreamer overlies a pair of filament systems (visible here in both H $\alpha$  and He II) and is bounded on each side by a dark helium coronal hole. Eclipse observations are from F. Espenak and M. Druckmüller (<http://www.zam.fme.vutbr.cz/~druck/Eclipse>).

In Figure 4, we present several more examples of pseudostreamers observed with the LASCO C2 coronagraph during the declining phase of solar cycle 23. The corresponding PFSS field-line topologies are displayed in Figure 5. In every case, the pseudostreamer overlies a double arcade that separates the polar coronal hole from a lower latitude hole of the same polarity (or from an equatorward extension of the polar hole). In general, because open flux is often present at the peripheries of active regions, pseudostreamers (like helmet streamers) may occur above activity complexes as well as over quiet areas of the solar surface.

As suggested by an inspection of Figure 4, the outer extensions of both pseudostreamers and helmet streamers consist of fine, radially oriented rays. Just as for a helmet streamer, the morphological appearance of a pseudostreamer in the LASCO C2 field of view depends on its orientation with respect to the observer: if the axis of the underlying double arcade is almost perpendicular to the limb, the white-light rays line up to form a bright, narrow spike; otherwise, they form a fainter and broader fan-shaped structure. The principal morphological difference between the two types of streamers in Figure 4 is that the helmet streamer cusps protrude above the LASCO C2 occulter, whereas only the long stalks of the pseudostreamers are visible above  $r \sim 2 R_{\odot}$ . Indeed, according to the PFSS model, the closed portion of a helmet streamer must extend out to  $r = R_{ss}$ ; if the cusp were

located at lower heights, a current sheet would necessarily be present between the cusp point and the source surface, violating the  $\nabla \times \mathbf{B} = 0$  assumption. In contrast, because a current sheet is not required along the boundary between open field lines of the same polarity, the cusp of a pseudostreamer may be located anywhere in the region  $R_{\odot} < r < R_{ss}$ .

Koutchmy et al. (1994) suggested that white-light streamer rays are jets, analogous to those detected in soft X-rays in the low corona by Shibata et al. (1992). However, even though density inhomogeneities (“blobs”) are observed moving continually outward along helmet streamer rays (Sheeley et al. 1997; Wang et al. 1998a), such gradually accelerating outflows do not have the impulsive character of jets. Figure 6 shows the difference between the LASCO C2 image recorded at 13:31 UT on 2005 August 8 (see Fig. 4c) and one taken 37 minutes earlier. In this difference image, the pseudostreamers at the northeast and southwest limbs are barely visible, indicating their quasi-steady nature; the helmet streamer at the southeast limb is also relatively quiescent at this time, while faint blobs may be seen moving outward along the plasma sheet extension of the face-on helmet streamer in the northwest quadrant. These outflows contrast with the jetlike events at position angle P.A.  $\sim 260^{\circ}$  and  $\sim 214^{\circ}$ . Such collimated ejections generally have EIT counterparts near the solar surface and appear to be triggered by magnetic reconnection between bipoles and neighboring open flux (see Wang et al. 1998b, 2006;

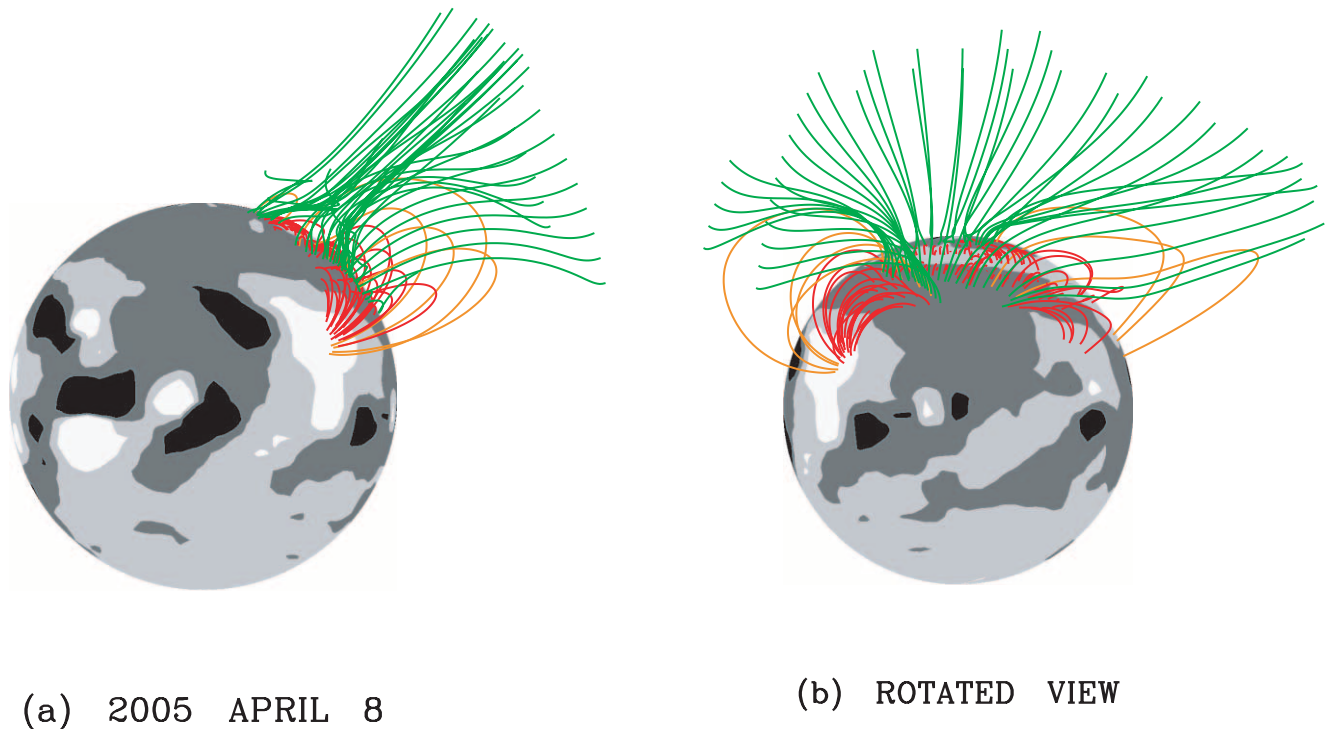


FIG. 2.—Field-line configuration of the pseudostreamer of Fig. 1 (a) as viewed from Earth on 2005 April 8, and (b) rotated by  $90^\circ$  in longitude. The coronal magnetic field was derived by applying a PFSS extrapolation with  $R_{ss} = 2.5 R_\odot$  to the MWO photospheric map for CR 2028. Here and in Fig. 5, open field lines are coded blue (green) if directed outward (inward); closed field lines are orange if they extend beyond  $r = 1.5 R_\odot$ , red otherwise. Black, dark gray, light gray, and white denote areas of the photosphere where  $B_r < -10$  G,  $-10$  G  $< B_r < 0$  G,  $0$  G  $< B_r < +10$  G, and  $B_r > +10$  G, respectively.

Dobrzycka et al. 2000, 2002; Wang & Sheeley 2002). The broad white-light jet in Figure 6 has its source in an active region located at the west limb just below the equator; the ejected material is channeled outward along the open field lines from the adjacent coronal hole (see Fig. 5c). The much narrower and fainter jet at

P.A. =  $214^\circ$  originates from a flaring Fe XII 19.5 nm bright point inside the south polar hole.

### 3. A MODEL FOR THE WHITE-LIGHT STREAMER BELT

The streamer belt beyond  $r \sim 2.5 R_\odot$  has previously been modeled as a thin plasma sheet centered on the HCS (Wang & Sheeley 1992; Wang et al. 1997; Liewer et al. 2001; Saez et al. 2005; Themisien & Howard 2006). We now modify this approach by including the effect of subsidiary plasma sheets associated with pseudostreamers. The outer streamer belt thus comprises two kinds of sheetlike density structures: the familiar heliospheric plasma sheet (HPS), whose base coincides with the source-surface neutral line where  $B_r(R_{ss}, L, \phi) = 0$ , and the pseudostreamer plasma sheets (PPS), which extend outward from the cusps of pseudostreamers. To locate the PPS, we proceed as follows. At equal intervals in longitude and latitude at the source surface, we trace downward along the magnetic field from  $r = R_{ss}$  to  $r = R_\odot$  and record the footpoint position and polarity of each field line. An arbitrary point  $(R_{ss}, L, \phi)$  on the source surface lies between four traced field lines. If at least two of these neighboring field lines have footpoint separations  $\Delta s > (\pi/12) R_\odot$  (say) and are of the same polarity, then the given point is taken to lie on a PPS (or boundary between open field regions of the same polarity). Having thus determined the angular locations of the PPS at the source surface, we assume for simplicity that both the PPS and the HPS extend radially outward in the region  $r > R_{ss}$ .

To derive the streamer patterns beyond  $r \sim 2.5 R_\odot$ , we suppose that the Thomson-scattering electrons are concentrated, at both the HPS and the PPS, within a layer of 1 pixel ( $4^\circ$ ) angular width. The arbitrarily normalized plasma densities are assigned values of 1.0 (HPS), 0.33 (PPS), and 0.1 (coronal hole) at  $r = R_{ss} = 2.5 R_\odot$ , and are assumed to fall off as  $r^{-2.5}$ . (Our choice of parameters



FIG. 3.—Outward extension of the pseudostreamer of Fig. 1, as observed with the LASCO C2 coronagraph at 07:27 UT on 2005 April 9. The contributions of the F corona and of instrumental stray light have been subtracted from the image, whose field of view extends from  $r \sim 2.2 R_\odot$  to  $r \sim 6 R_\odot$ . The axis of the underlying double arcade is oriented perpendicular to the sky plane, so that the pseudostreamer rays line up to form a narrow stalk.

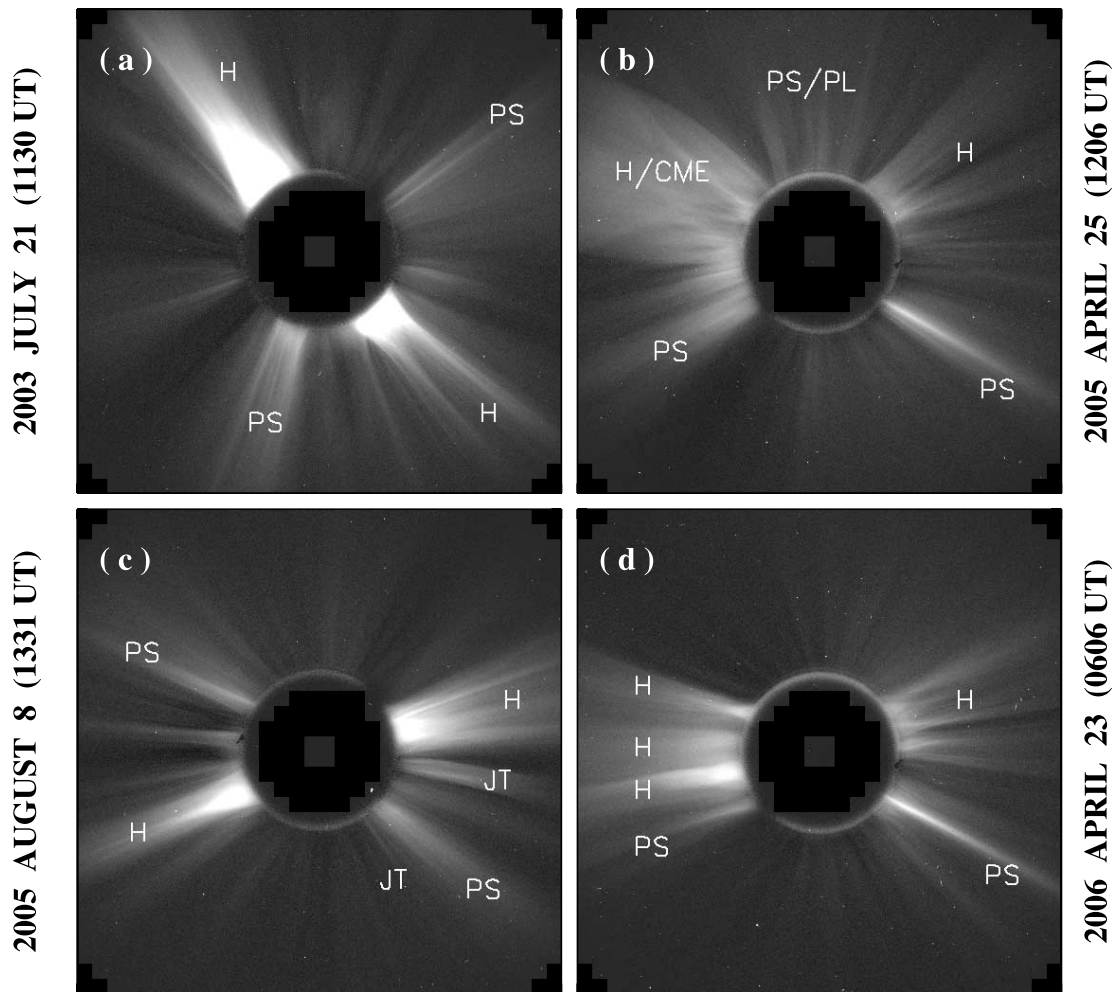


FIG. 4.—Background-subtracted LASCO C2 images showing examples of pseudostreamers during the declining phase of solar cycle 23. (a) 2003 July 21 (11:30 UT). (b) 2005 April 25 (12:06 UT). (c) 2005 August 8 (13:31 UT). (d) 2006 April 23 (06:06 UT). Occulting disk extends out to  $r \sim 2.2 R_{\odot}$ . Labels identify white-light structures as pseudostreamers (“PS”), helmet streamers (“H”), or jets (“JT”); in addition, “PS/PL” denotes a mixture of pseudostreamers and polar plumes, while “H/CME” designates a helmet streamer blowout.

is illustrative and intended only to capture the qualitative appearance of the observed brightness patterns.) The distribution of the scattered photospheric radiation is then calculated as a function of sky plane position using the formulae of Billings (1966).

We illustrate the model by simulating the observed streamer structures during CR 2005 (starting date 2003 July 6). The Carrington-format maps of Figure 7 show the distribution of He I 1083.0 nm coronal holes, the PFSS-derived neutral line and boundaries between like-polarity holes at  $r = R_{ss}$ , the LASCO C2 brightness patterns at  $r = 3.0 R_{\odot}$ , and the simulated streamer patterns. The C2 synoptic map was assembled from successive strips of west limb data recorded over the 27.3 day rotation period.

From Figure 7b, we note that the “pseudostreamer lines” that separate holes of the same polarity branch off the source-surface neutral line, rather like the tributaries of a river. At those longitudes where the hole boundaries run horizontally (vertically), the HPS or PPS is oriented edge-on (face-on) when viewed in the sky plane. The arc-shaped structures in the observed and simulated intensity maps are traced out by edge-on streamers as they rotate past the Sun’s limb, where they reach their minimum apparent latitude (corresponding to their actual  $L$ ). In accordance with the LASCO observations, the brightest of the simulated arcs are associated with the HPS, to which we have assigned higher

plasma densities than to the PPS. The two pseudostreamers observed on 2003 July 21 are identified by arrows in Figures 7c and 7d (cf. Figs. 4a and 5a).

Figures 8 through 10 display the observed and simulated streamer patterns for CR 2028, 2033, and 2042, whose respective starting dates are 2005 March 25, 2005 August 8, and 2006 April 10. The top left panel in each figure shows the underlying distribution of Fe xv 28.4 nm emission recorded by EIT, in which dark areas represent coronal holes (no NSO He I 1083.0 nm synoptic maps were available for this period). The pseudostreamers of 2005 April 9 and 25, August 8, and 2006 April 23 are marked by arrows in both the observed and simulated streamer maps (cf. Figs. 3, 4b, 4c, and 4d). We note that the topology of the source-surface neutral line (HCS/HPS) has evolved from a two-sector tilted dipole during 2003 to a four-sector quadrupole during 2005–2006. Again, including the effect of scattering from the multiple PPS improves the agreement between the calculated and observed white-light patterns.

#### 4. DISCUSSION

In our study of the 2006 March 29 solar eclipse (Wang et al. 2007), we concluded that the narrow linear features permeating the outer corona fall into three categories: (1) plumes that overlie small bipoles inside coronal holes, (2) helmet streamer rays that

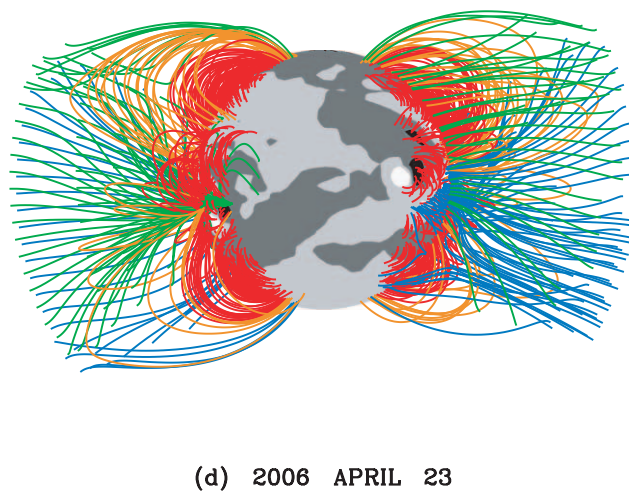
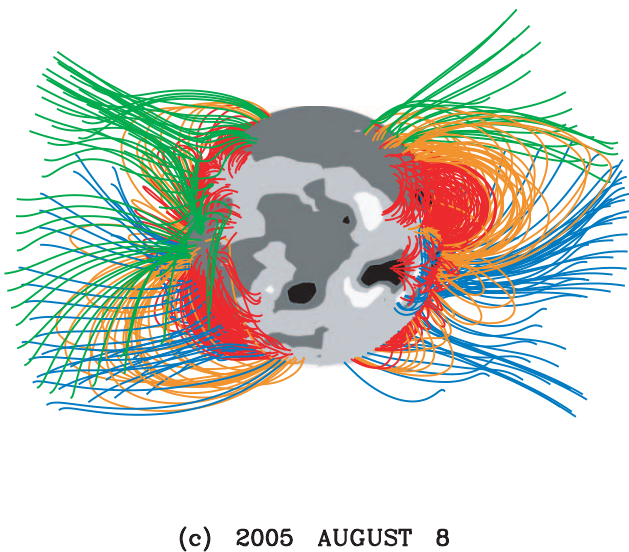
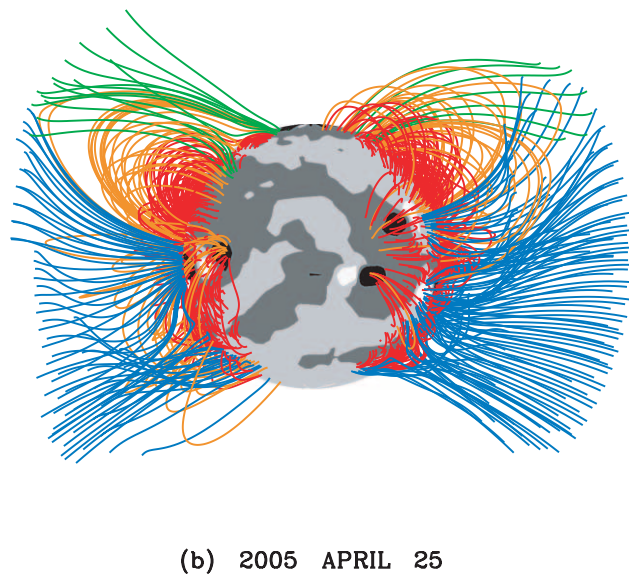
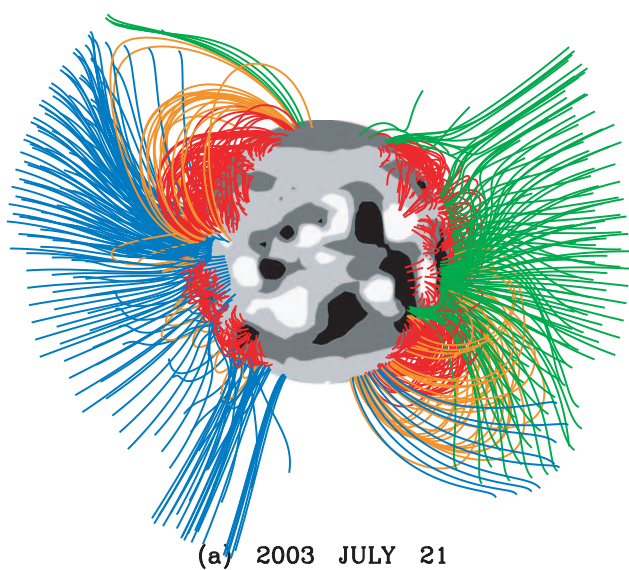


FIG. 5.—Field-line topologies of the streamer structures in Fig. 4. (a) 2003 July 21. (b) 2005 April 25. (c) 2005 August 8. (d) 2006 April 23. For color key, see Fig. 2 legend. The coronal configurations were derived by applying a PFSS extrapolation to the MWO photospheric field maps for CR 2005, 2029, 2033, and 2042, respectively. For clarity, we have plotted only field lines within  $45^\circ$  of either limb, and only those open field lines that are rooted next to closed loops.

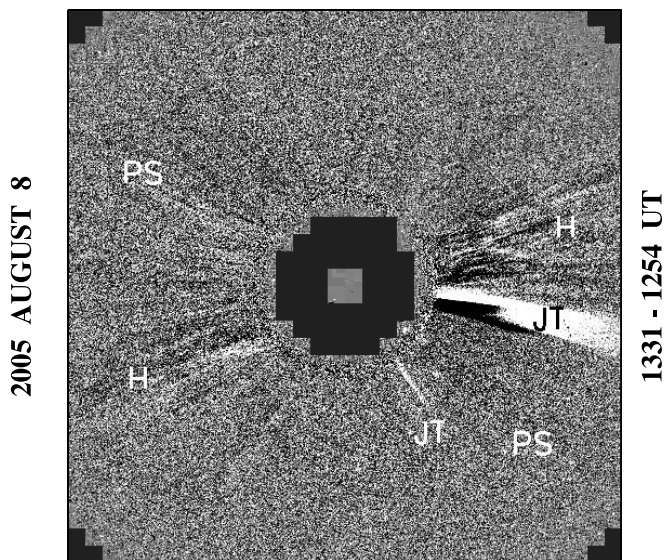


FIG. 6.—Difference between the LASCO C2 image of Fig. 4c and one recorded 37 minutes earlier at 12:54 UT on 2005 August 8. White (black) indicates that the coronal brightness or electron density has increased (decreased) during the intervening time. Faint blobs may be seen streaming outward along the plasma sheet extension of the face-on helmet streamer in the northwest quadrant. More striking are the two jets in the southwest quadrant; such fast, collimated ejections are triggered by interactions between emerging bipoles and coronal holes, and are frequently observed in the vicinity of pseudostreamers. In contrast, the pseudostreamers themselves are relatively quiescent and are barely visible in this difference image.

overlie loop arcades separating coronal holes of opposite polarity, and (3) pseudostreamer rays that overlie double arcades separating coronal holes of the same polarity. We also proposed that, in all cases, the rays are produced by magnetic reconnection between the underlying closed loops and the adjacent coronal-hole field lines. As a result of such footpoint exchanges or “interchange reconnection” (Nash et al. 1988; Fisk & Schwadron 2001; Crooker et al. 2002; Wang & Sheeley 2004; Lionello et al. 2005), material trapped inside the loops is continually released into the heliosphere. Evidence for interchange reconnection in helmet streamers is provided by the small plasma blobs that are extruded from their cusps and accelerate outward along the HPS (Sheeley et al. 1997; Wang et al. 1998a).

The cusp of a pseudostreamer coincides with an  $X$ -type neutral point, where the two open and two closed flux systems come into mutual contact. (A helmet streamer cusp corresponds to a  $Y$ -type neutral point; see, e.g., Sturrock & Smith 1968.) Here, two types of interchange reconnection may occur. First, analogous to the process that gives rise to helmet streamer rays, a closed loop may undergo three-dimensional reconnection with an open field line rooted next to it. Second, the closed loop may reconnect with an open field line rooted in the other coronal hole, resulting in the transfer of open and closed flux in opposite directions across the  $X$ -point. The latter process is similar to that which triggers jets when bipoles emerge inside coronal holes (see, e.g., Shibata et al. 1992; Wang et al. 2006). As remarked in § 2, however, pseudostreamers do not have the impulsive characteristics of LASCO white-light jets, whose leading edges propagate outward with speeds ranging from  $\sim 400$  to over  $1000 \text{ km s}^{-1}$  (Wang et al. 1998b; Wang & Sheeley 2002). The quasi-steady behavior of pseudostreamers more closely resembles that of large-scale coronal plumes. The elevated densities in plumes requires strong, persistent heating to be present near their bases (Wang 1994a). The most likely source of this enhanced heating is continual  $X$ -point

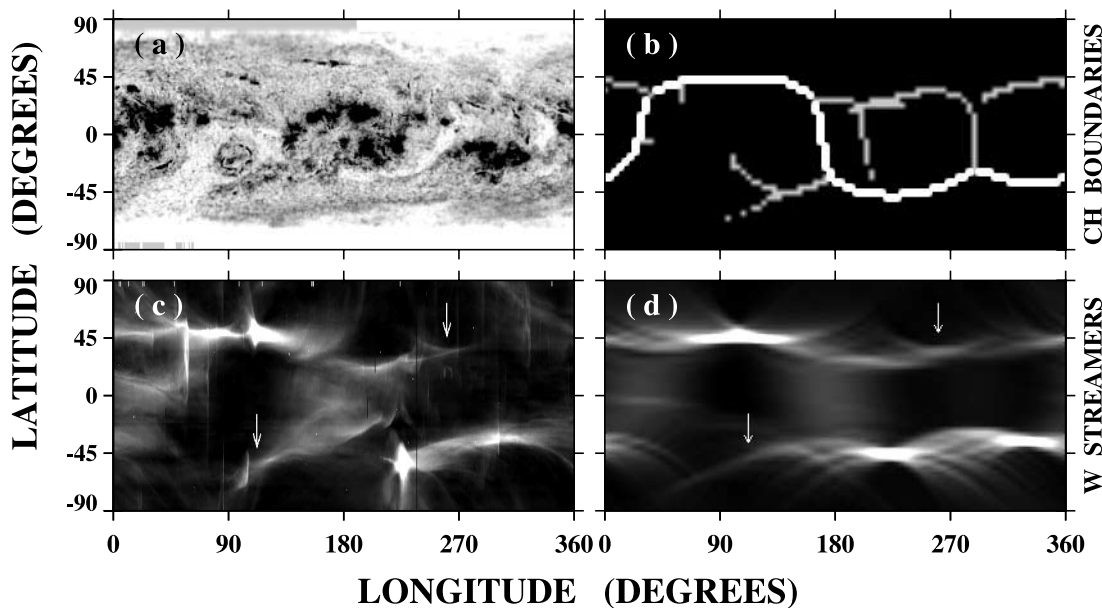


FIG. 7.—Latitude-longitude maps for CR 2005 (starting date 2003 July 6), showing (a) the distribution of He I 1083.0 nm intensities, (b) the boundaries between open field regions at  $r = R_{ss} = 2.5 R_{\odot}$ , (c) the LASCO C2 brightness patterns at the west limb, and (d) the corresponding simulated streamer structures. In the National Solar Observatory (NSO) helium map, coronal holes (active regions) appear as white (black) areas. In the source surface map, the heavy white line represents the heliospheric current/plasma sheet, which separates holes of opposite polarity; gray lines mark the locations of pseudostreamer plasma sheets, which separate holes of the same polarity. The coronal brightness map was constructed by extracting strips of west limb data centered at  $r = 3 R_{\odot}$  from background-subtracted LASCO C2 images and arranging the strips in a time-reversed sequence. The simulated streamer patterns were produced by Thomson scattering of photospheric radiation from the heliospheric and pseudostreamer plasma sheets, whose respective internal densities were taken to be in the ratio 3:1. In both the observed and simulated white-light maps, the pseudostreamers of 2003 July 21 are identified by arrows (compare Fig. 4a).

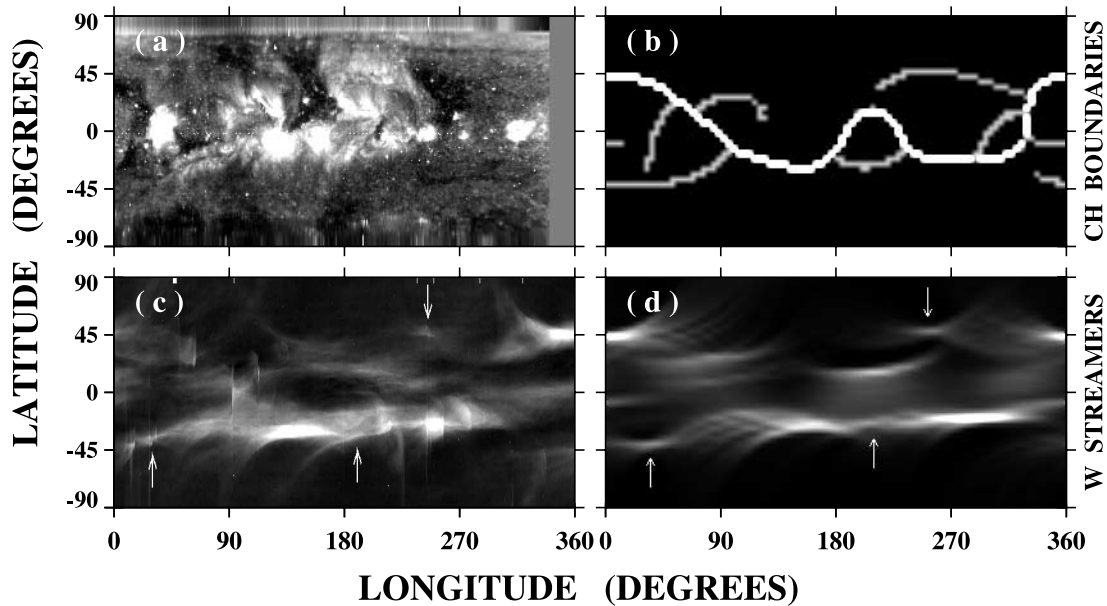


FIG. 8.—Latitude-longitude maps for CR 2028 (starting date 2005 March 25), showing (a) the distribution of Fe xv 28.4 nm intensities, (b) the boundaries between open field regions at the source surface, (c) the LASCOC2 brightness patterns at the west limb, and (d) the corresponding simulated streamer structures. In the EIT synoptic map, coronal holes (active regions) appear as black (white) areas. Arrows point to the northern-hemisphere pseudostreamer of Fig. 3 and to the two southern-hemisphere pseudostreamers of Fig. 4b.

reconnection between the small underlying bipoles and the open flux associated with the unipolar flux concentrations within the coronal hole (Wang 1998, and references therein). The characteristic  $\sim 1$  day lifetime of a plume is determined by the decay timescale of an ephemeral region in the supergranular flow field. In contrast, because they overlie larger loop arcades, pseudostreamers may persist for months instead of days.

Empirical studies have shown that the rate of flux tube expansion in the corona is inversely correlated with the solar wind speed at 1 AU (Levine et al. 1977; Wang & Sheeley 1990; Arge & Pizzo 2000). The open flux near the boundary between coronal holes of opposite polarity diverges rapidly with height, since  $B_r \rightarrow 0$  at the source-surface neutral line; thus, the helmet

streamer rays and their plasma sheet extension are associated with very slow wind. In contrast, the flux tubes at the boundary between holes of the same polarity are characterized by low expansion factors, since the outward-fanning field lines from the two holes “repel” each other and are diverted into a more radial direction (see Sheeley & Wang 1991). Thus, we expect pseudostreamers to be sources of high-speed wind. Indeed, given that they are far brighter and longer lived than polar plumes, pseudostreamers and their plasma sheet extensions may provide the best available means—as yet unexploited—to observe the fast solar wind near its origin, just as helmet streamers and their plasma sheet extensions allow us to probe the acceleration of the slow solar wind.

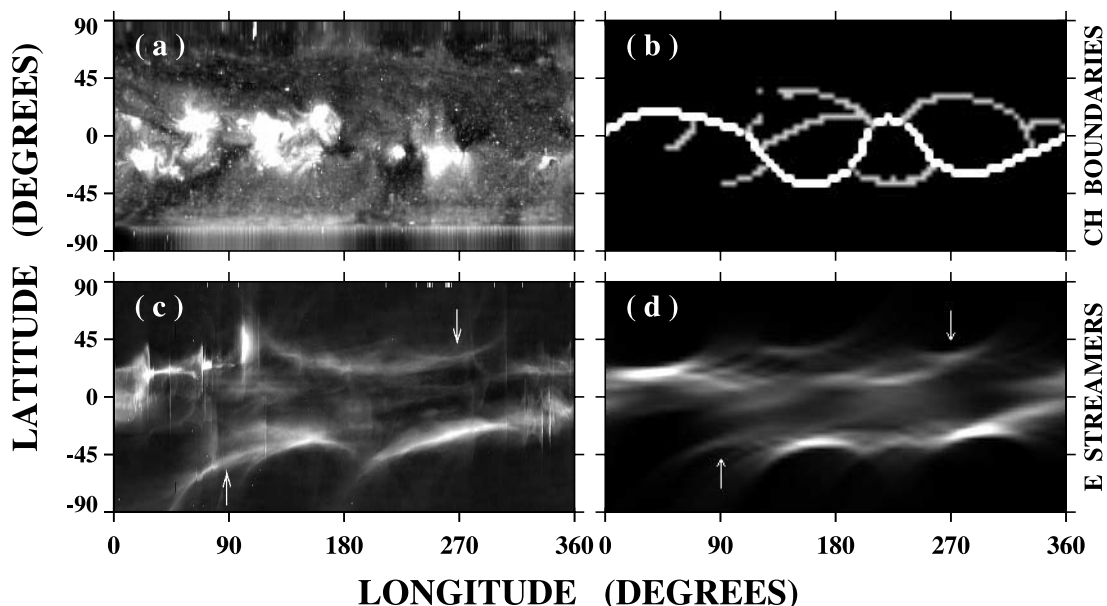


FIG. 9.—Latitude-longitude maps for CR 2033 (starting date 2005 August 8), showing (a) the distribution of Fe xv 28.4 nm intensities, (b) the boundaries between open field regions at the source surface, (c) the LASCOC2 brightness patterns at the east limb, and (d) the corresponding simulated streamer structures. Arrows identify the pseudostreamers of Fig. 4c during their east limb passage.

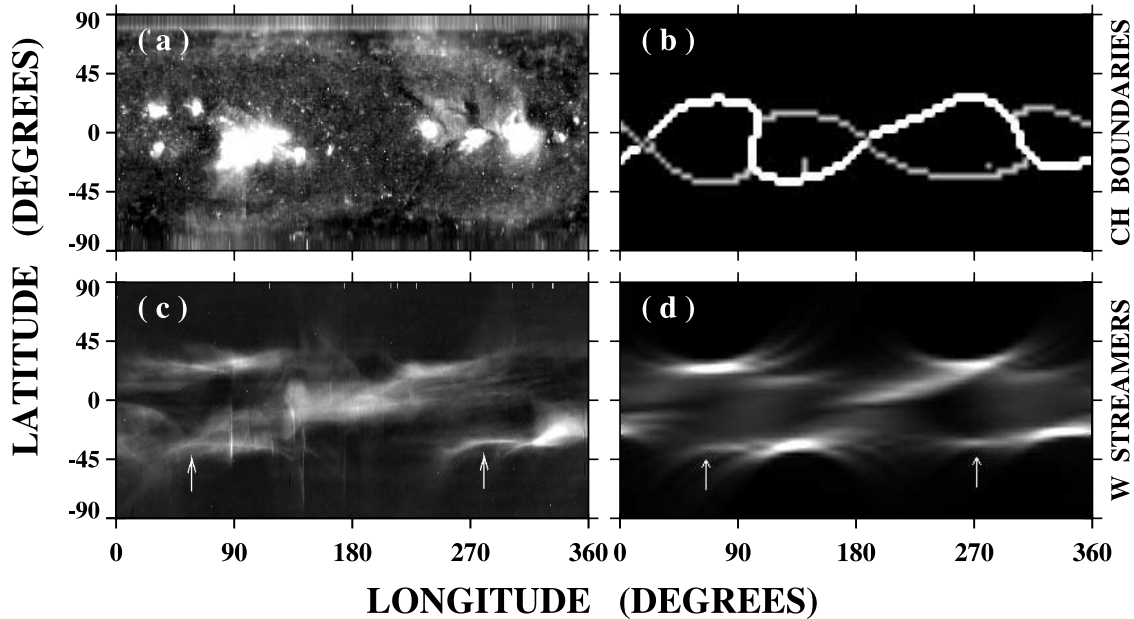


FIG. 10.—Latitude-longitude maps for CR 2042 (starting date 2006 April 10) showing (a) the distribution of Fe xv 28.4 nm intensities, (b) the boundaries between open field regions at the source surface, (c) the LASCO C2 brightness patterns at the west limb, and (d) the corresponding simulated streamer structures. Arrows identify the pseudostreamers of Fig. 4d during their west limb passage.

Figure 11a shows a height-time map of the outflows above a pseudostreamer. Here, a radial strip aligned along the pseudostreamer axis was extracted from each of a succession of LASCO C2 and C3 running-difference images, and the vertically oriented strips were then arranged in a time-ordered sequence. The pseudostreamer in question is that located at P.A.  $\simeq 240^\circ$  on 2006 April 23 and displayed in Figure 4d; it also appears as a narrow, horizontal feature at  $\phi \sim 280^\circ$  in the observed and simulated

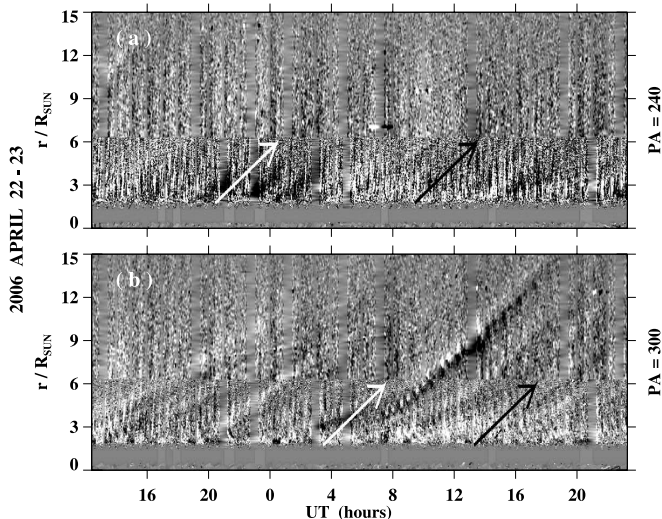


FIG. 11.—Height-time maps showing the outflows during 2006 April 22–23 (a) above a pseudostreamer and (b) above a helmet streamer. For reference, arrows indicate the slope corresponding to a constant radial flow speed of  $200 \text{ km s}^{-1}$  (or  $1 R_\odot \text{ hr}^{-1}$ ). The streamers are located at P.A.  $\sim 240^\circ$  and P.A.  $\sim 300^\circ$ , respectively, and appear at the west limb in Fig. 4d. The maps were constructed from LASCO C2 and C3 running-difference images, by excising from each image a radial strip centered on the streamer axis and arranging the strips in a time-ordered sequence. The pseudostreamer outflows appear as faint, straight tracks roughly parallel to the arrows but no longer detectable beyond  $r \sim 6 R_\odot$ . In contrast, the helmet streamer blobs (emerging after  $\sim 0$  UT) form long, upward curving tracks, whose slopes in the middle of the C2 field of view correspond to velocities well below  $200 \text{ km s}^{-1}$ .

white-light streamer maps for CR 2042 (Figs. 10c and 10d). The height-time display reveals a succession of faint, straight tracks traversing the C2 field of view but no longer detectable above  $r \sim 6 R_\odot$ , probably because of the low sensitivity of the C3 coronagraph. As indicated by the superimposed fiducial arrows, the slopes of the tracks correspond to characteristic speeds as high as  $200 \text{ km s}^{-1}$  at heliocentric distances as small as  $\sim 3 R_\odot$ . For comparison, Figure 11b shows the outflows above a helmet streamer at P.A.  $\simeq 300^\circ$  during the same period. In this case, a series of upward curving tracks representing streamer blobs may be seen traversing the C2 and C3 fields of view during April 23. These blobs typically have velocities well below  $100 \text{ km s}^{-1}$  at  $r \sim 3 R_\odot$  and have been interpreted by Sheeley et al. (1997) as being swept along like leaves by the ambient slow solar wind. The velocities inferred from the height-time maps of Figure 11 are consistent with solar wind energy-balance models in which the sonic point is located at  $r \sim 2\text{--}3 R_\odot$  in high-speed flows, but at  $r \sim 5\text{--}6 R_\odot$  in slow wind (see, e.g., Wang 1994a, 1994b).

We note that the PFSS model does not correctly describe the magnetic topology beyond  $r \sim 2.5 R_\odot$ , where the flux distribution in reality becomes increasingly uniform in  $L$  and  $\phi$ . In particular, the like-polarity open field lines that converge above pseudostreamers subsequently diverge again in order to maintain transverse pressure balance. Conversely, the rapidly diverging flux tubes at the boundaries between opposite-polarity coronal holes subsequently reconverge in solid angle, so that  $\mathbf{B}$  suddenly reverses its direction at the HCS rather than going gradually through zero. This refocusing of the plasma flow above the cusps of helmet streamers at least partly accounts for the tendency for the HPS to dominate the brightness of the outer corona and to survive as a well-defined structure at 1 AU (see Borrini et al. 1981; Winterhalter et al. 1994; Crooker et al. 2004).

We are indebted to the *SOHO* LASCO and EIT teams for the use of their observations; we also thank R. K. Ulrich for providing the MWO photospheric field data. This work was supported by NASA and the Office of Naval Research.

## REFERENCES

- Arge, C. N., Hildner, E., Pizzo, V. J., & Harvey, J. W. 2002, *J. Geophys. Res.*, 107, A10, SSH 16-1
- Arge, C. N., & Pizzo, V. J. 2000, *J. Geophys. Res.*, 105, 10465
- Billings, D. E. 1966, *A Guide to the Solar Corona* (New York: Academic)
- Borrini, G., Gosling, J. T., Bame, S. J., Feldman, W. C., & Wilcox, J. M. 1981, *J. Geophys. Res.*, 86, 4565
- Brueckner, G. E., et al. 1995, *Sol. Phys.*, 162, 357
- Burlaga, L. F., Hundhausen, A. J., & Zhao, X. 1981, *J. Geophys. Res.*, 86, 8893
- Crooker, N. U., Gosling, J. T., & Kahler, S. W. 2002, *J. Geophys. Res.*, 107, A2, SSH 3-1
- Crooker, N. U., Huang, C. -L., Lamassa, S. M., Larson, D. E., Kahler, S. W., & Spence, H. E. 2004, *J. Geophys. Res.*, 109, A03107
- Delaboudinière, J. -P., et al. 1995, *Sol. Phys.*, 162, 291
- Dobrzycka, D., Cranmer, S. R., Raymond, J. C., Biesscker, D. A., & Gurman, J. B. 2002, *ApJ*, 565, 621
- Dobrzycka, D., Raymond, J. C., & Cranmer, S. R. 2000, *ApJ*, 538, 922
- Fisk, L. A., & Schwadron, N. A. 2001, *ApJ*, 560, 425
- Gosling, J. T., Borrini, G., Asbridge, J. R., Bame, S. J., Feldman, W. C., & Hansen, R. T. 1981, *J. Geophys. Res.*, 86, 5438
- Hansen, S. F., Sawyer, C., & Hansen, R. T. 1974, *Geophys. Res. Lett.*, 1, 13
- Howard, R. A., & Koomen, M. J. 1974, *Sol. Phys.*, 37, 469
- Koutchmy, S., Koutvitsky, V. A., Molodensky, M. M., Solov'iev, L. S., & Koutchmy, O. 1994, *Space Sci. Rev.*, 70, 283
- Levine, R. H., Altschuler, M. D., & Harvey, J. W. 1977, *J. Geophys. Res.*, 82, 1061
- Liewer, P. C., et al. 2001, *J. Geophys. Res.*, 106, 15903
- Lionello, R., Riley, P., Linker, J. A., & Mikić, Z. 2005, *ApJ*, 625, 463
- Nash, A. G., Sheeley, N. R., Jr., & Wang, Y. -M. 1988, *Sol. Phys.*, 117, 359
- Pneuman, G. W., Hansen, S. F., & Hansen, R. T. 1978, *Sol. Phys.*, 59, 313
- Saez, F., Zhukov, A. N., Lamy, P., & Llebaria, A. 2005, *A&A*, 442, 351
- Schatten, K. H., Wilcox, J. M., & Ness, N. F. 1969, *Sol. Phys.*, 6, 442
- Sheeley, N. R., Jr., & Wang, Y. -M. 1991, *Sol. Phys.*, 131, 165
- Sheeley, N. R., Jr., et al. 1997, *ApJ*, 484, 472
- Shibata, K., et al. 1992, *PASJ*, 44, L173
- Sturrock, P. A., & Smith, S. M. 1968, *Sol. Phys.*, 5, 87
- Thermisien, A. F., & Howard, R. A. 2006, *ApJ*, 642, 523
- Ulrich, R. K., Evans, S., Boyden, J. E., & Webster, L. 2002, *ApJS*, 139, 259
- Wang, Y. -M. 1994a, *ApJ*, 435, L153
- . 1994b, *ApJ*, 437, L67
- . 1998, *ApJ*, 501, L145
- Wang, Y. -M., Bierstecker, J. B., Sheeley, N. R., Jr., Koutchmy, S., Mouette, J., & Druckmüller, M. 2007, *ApJ*, in press
- Wang, Y. -M., Pick, M., & Mason, G. M. 2006, *ApJ*, 639, 495
- Wang, Y. -M., & Sheeley, N. R., Jr. 1990, *ApJ*, 355, 726
- . 1992, *ApJ*, 392, 310
- . 1995, *ApJ*, 447, L143
- . 2002, *ApJ*, 575, 542
- . 2004, *ApJ*, 612, 1196
- Wang, Y. -M., Sheeley, N. R., Jr., Socker, D. G., Howard, R. A., & Rich, N. B. 2000, *J. Geophys. Res.*, 105, 25133
- Wang, Y. -M., et al. 1997, *ApJ*, 485, 875
- . 1998a, *ApJ*, 498, L165
- . 1998b, *ApJ*, 508, 899
- Wilcox, J. M., & Hundhausen, A. J. 1983, *J. Geophys. Res.*, 88, 8095
- Winterhalter, D., Smith, E. J., Burton, M. E., Murphy, N., & McComas, D. J. 1994, *J. Geophys. Res.*, 99, 6667